Aging-induced metal redistribution in bimetallic catalysts

G.W. Graham [a]*, H. Sun [b], H.-W. Jen [a], X.Q. Pan [b], and R.W. McCabe [a]

[a] *Chemical Engineering Department, Ford Research Laboratory, MD3179/SRL, PO Box 2053, Dearborn, MI 48121, USA*
[b] *Department of Materials Science and Engineering, University of Michigan, 2300 Hayward Street, Ann Arbor, MI 48109-2136, USA*

Received 20 October 2001; accepted 8 January 2002

Alloy particles were detected by XRD in bimetallic catalysts, made from physical mixtures of powders comprising distinct metal–support combinations (*e.g.*, Pd on alumina and Rh on ceria–zirconia), following high-temperature redox aging. The morphology of the catalysts was examined by TEM, and the compositional structure of some of the alloy particles was determined. Two different effects of the redistribution of metals on oxygen-storage capacity were identified, one due to Pd enrichment of the surface of Pd–Rh alloy particles and the other due to loss of contact between metal and ceria–zirconia.

KEY WORDS: aging; alloying; automotive exhaust catalysts; bimetallic catalysts; ceria–zirconia; oxygen storage; Pd–Rh; Pt–Rh; TEM.

1. Introduction

Improvements in the thermal stability of three-way catalysts, used for treating automotive exhaust, are sought because they should lead to lower emissions and better fuel economy. A major advance in this area came from the recent development of high-surface-area ceria–zirconia, a remarkable oxygen-storage material that can also serve as a support for the catalytically-active precious metal [1,2]. Consequently, the metal–support contact necessary for realizing oxygen storage is naturally maintained as both the metal and the support undergo sintering.

The importance of establishing certain desirable metal–support associations is well known in automotive catalysis. Recognition of the deleterious interaction between Rh and γ-alumina under oxidizing conditions [3], for example, led to the idea of supporting Rh on zirconia, which is less reactive [4]. The maintenance of particular metal–support associations may be compromised, however, if other high-surface-area materials are present in the catalyst *and* the metal is able to migrate from one support to the other [5]. In multimetallic catalysts, where two or more distinct metal–support combinations are present initially, such metal transport could also lead to the formation of alloys that have different catalytic properties than their constituents.

The potential for problems associated with metal transport (beyond just the reduction in metal surface area) has certainly been recognized in the past, but metal transport is likely to be more prevalent at the higher temperatures of current interest. Further, the advance in thermal stability of three-way catalysts, derived from high-surface-area ceria–zirconia, was based to a large extent on Pd-only formulations for which alloying was not a consideration [6]. Rising Pd prices have prompted renewed interest in Pt–Rh, Pd–Rh and Pt–Pd–Rh formulations, however. Thus, the present investigation of some model bimetallic catalysts was undertaken to probe for possible effects of metal redistribution at high temperature. The results indicate that such effects could be significant.

2. Experimental aspects

Three model bimetallic catalysts, one Pt–Rh and two Pd–Rh formulations, were made by physically mixing previously prepared single-metal catalyst powders. The various constituents and mixtures are listed in table 1. Four of the single-metal catalysts, PtI, RhI, RhII and PdI, were made using a commercially-feasible ceria–zirconia support material from Rhodia, CZ3 [1], while the fifth single-metal catalyst, PdII, was made using a commercial La-stabilized alumina from W.R. Grace, MI380. Powder particle size of all the single-metal catalysts is in the range 10–35 μm. The Pt–Rh catalyst, PtI + RhI, has an overall metals ratio of four parts Pt to one part Rh by weight (or a molar ratio of about two parts Pt to one part Rh), whereas the Pd–Rh catalysts, PdI + RhII and PdII + RhII, both have overall metal ratios of one part Pd to one part Rh by weight. Aging (specifically, *redox* aging) was performed by heating the powders, supported within a quartz boat, in a tube furnace at 1050 °C for 12 h under a gas mixture which alternated every 10 min between reducing (1% CO/H_2) and oxidizing (0.5% O_2), the balance in each case consisting of 10% H_2O and 20 ppm SO_2 in N_2. After aging, all three bimetallic catalysts were characterized by X-ray diffraction (XRD), using a Scintag X2 diffractometer with Cu K_α radiation, and the Pd–Rh catalysts were

* To whom correspondence should be addressed.

1011-372X/02/0700-0001/0

Table 1
Constituent materials, single-metal catalysts, and bimetallic catalysts

Material or catalyst	Designation	Description	BET area (m^2/g)	
			Fresh	Aged
CZ3		70 wt% CeO_2–30 wt% ZrO_2	(79)	7.1
2 wt% Pt/CZ3	PtI	Powder catalyst	(79)	(7.4)
0.5 wt% Rh/CZ3	RhI	Powder catalyst	(79)	(7.4)
2 wt% Rh//CZ3	RhII	Powder catalyst	(79)	(7.4)
2 wt% Pd/CZ3	PdI	Powder catalyst	79	7.4
MI380		γ-Al_2O_3	177	84
4 wt% Pd/MI380	PdII	Powder catalyst	177	(84)
	PtI + RhI	1 : 1 (wt : wt) mixture of PtI and RhI	(79)	(7.4)
	PdI + RhII	1 : 1 (wt : wt) mixture of PdI and RhII	(79)	(7.4)
	PdII + RhII	1 : 2 (wt : wt) mixture of PdII and RhII	(59 + 53)	(28 + 5)

further examined by transmission electron microscopy (TEM), using a JEOL 2010F electron microscope equipped with an X-ray energy-dispersive spectroscopy (EDS) system. Samples for TEM were prepared by contacting the dry powders with carbon-coated Cu grids. Oxygen storage capacity (OSC) measurements were performed on some of the samples after aging, utilizing alternating pulses of CO and O_2 in a microreactor, described previously [1]. Specific surface areas (BET) of some of the samples, measured with a Micromeritics ASAP 2400 instrument, are also listed in table 1. Numbers in parentheses were inferred from the measured values and, in the case of PdII + RhII, the two distinct support materials were regarded separately when inferring their contributions to the totals.

3. Results

The XRD pattern obtained from PtI + RhI after aging is shown in figure 1(a). In addition to the peaks due to ceria–zirconia, there is one set of precious-metal-derived peaks apparent, and these clearly fall between those of pure Pt and pure Rh [7]. In fact, the lattice constant is close to the molar-weighted-average (based on Pt : Rh of approximately 2 : 1) of the Pt and Rh lattice constants, as indicated by the (111) peak position in an expanded view shown in figure 1(b). (The small peak centered at 41.65° is from ceria–zirconia [7].) According to estimates based on the Scherrer equation, the dimensions of both the precious-metal and ceria–zirconia primary particles are at least several tens of nanometers.

In contrast to this, the XRD pattern obtained from PdI + RhII after aging, shown in figure 2(a), exhibits a relatively small peak near the position of the Rh (111) peak. However, reduction (performed in 1% H_2 at 300 °C for 30 min) of the aged catalyst results in a larger peak about halfway between the positions of the Pd (111) and Rh (111) peaks [7], as shown in figure 2(b). The dimensions of the precious-metal primary particles, again according to estimates based on the Scherrer

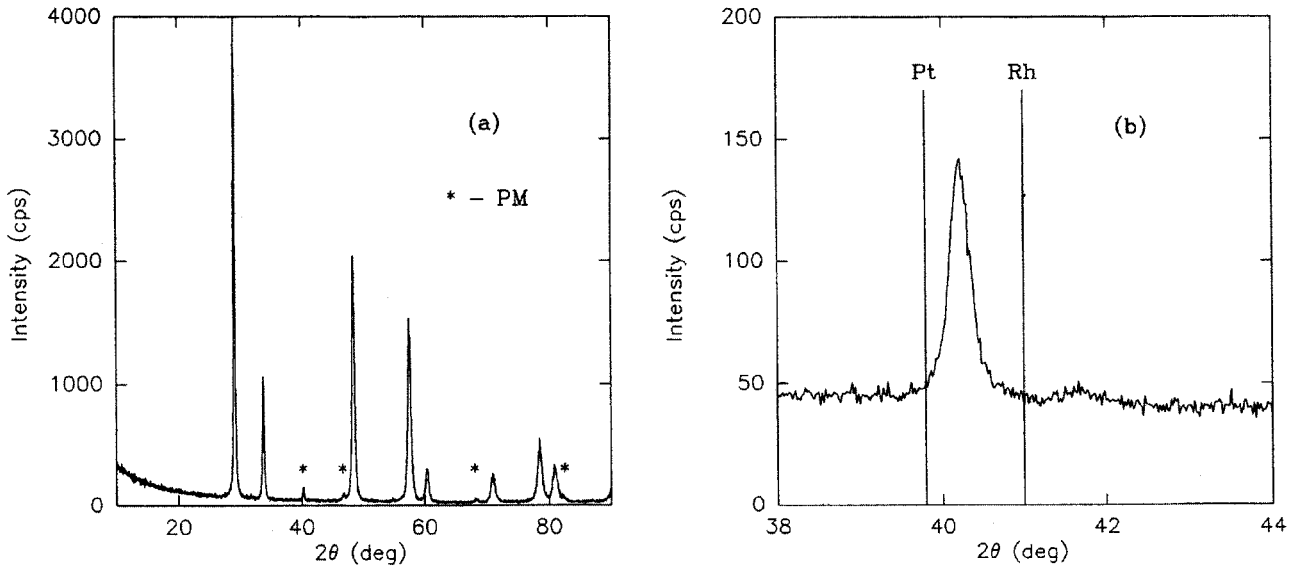

Figure 1. XRD patterns obtained from PtI + RhI after aging. The peaks marked with an asterisk in (a) are due to precious metal (PM).

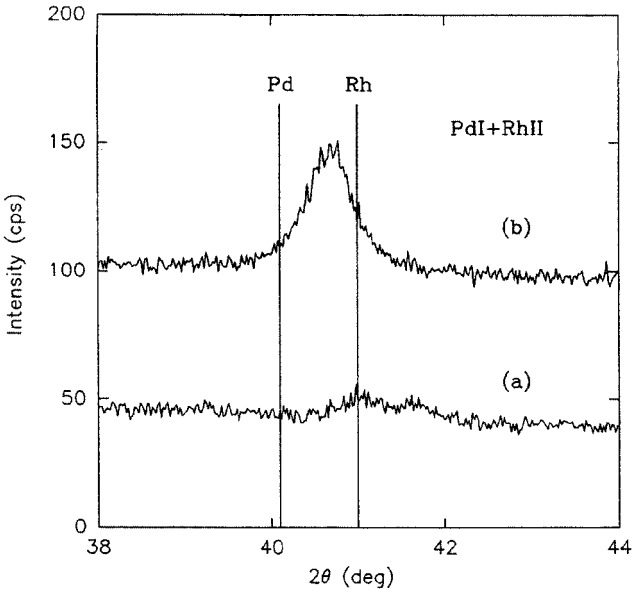

Figure 2. XRD patterns obtained from PdI + RhII after aging (a), followed by mild reduction (b).

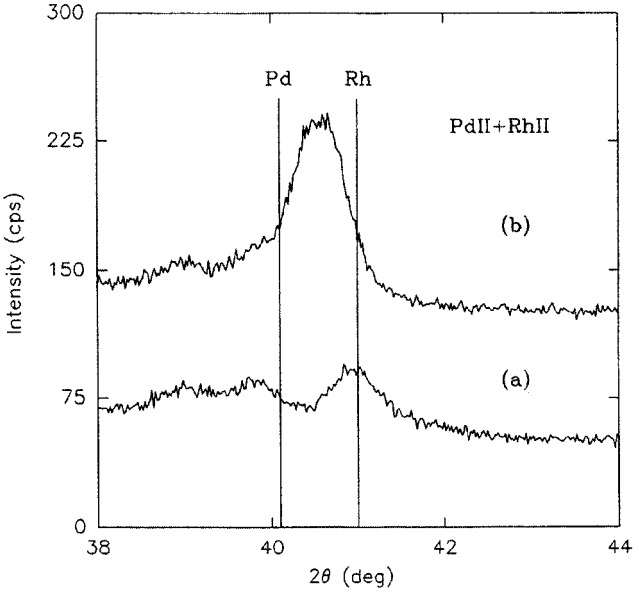

Figure 3. XRD patterns obtained from PdII + RhII after aging (a), followed by mild reduction (b).

equation, are smaller than before, only a few tens of nanometers. Similar behavior was found in the case of PdII + RhII, as shown in figure 3. A relatively small peak near the position of the Rh (111) peak after aging was replaced by a larger peak about halfway between the positions of the Pd (111) and Rh (111) peaks following the mild reduction treatment. (The peaks centered at 39° and 39.8° are from the alumina, which contains a mixture of δ- and θ-phases after aging [7].) Although there is no sign of a PdO (110) peak at 42° in figure 3(a), a small peak found near 54.8° (results not shown) could be from PdO (112) [7]. The reduction treatment removed this peak, and an oxidation treatment (performed in air at 700 °C for 2 h) slightly increased its intensity, while having no perceptible effect on the XRD pattern shown in figure 3(a). A more aggressive oxidation treatment (performed in air at 800 °C for 2 h) reduced the size of the peak at 41° in figure 3(a) by about 30%, but no Rh-containing oxide (*e.g.*, Rh_2O_3 or $PdRhO_2$) was detected by XRD [7].

A TEM image, taken from PdI + RhII following the mild reduction treatment performed after aging, is shown in figure 4(a). Although not apparent from the image, the EDS results shown in figure 4(b) reveal that both Pd and Rh are present in region 1 but not in region 2. A higher magnification image of region 1 is shown in figure 4(c), but the high-resolution (1 nm) EDS results, shown in figure 4(d), are needed in order to locate the source of the Pd and Rh signals, both of which appear to be coming from only the central portion of this image. The dimensions of individual ceria–zirconia grains, which are distinct but in close contact with each other, are consistent with the XRD estimates.

The TEM image shown in figure 5(a), taken from PdII + RhII following the mild reduction treatment performed after aging, reveals the morphology of the alumina. Also contained in this image, according to the EDS results shown in figure 5(b), are some ceria–zirconia grains (2, 3 and 4) and one precious-metal particle (1), which exhibits much better contrast against alumina than against ceria–zirconia (as in PdI + RhII). In this case, it is clear that the particle contains both Pd and Rh, and their distribution is fairly homogeneous, according to the EDS results shown in figure 5(d), taken from the enlarged image shown in figure 5(c). Not all of the particles are as homogeneous, however, and their compositions are not all the same, as shown by the results in figure 6, also taken from PdII + RhII. Here, the ratio of Pd to Rh peak heights varies between 0.33 (point 5) and 0.83 (point 3), compared with a ratio of about 1.2 in figure 5(d). Electron diffraction further reveals that such particles contain several crystallites, the dimensions of which would then be consistent with the XRD estimates (which apply to coherently-diffracting entities).

The effect of the 700 °C oxidation treatment on precious-metal particles in PdII + RhII was also examined by TEM. As illustrated by the image and accompanying EDS results shown in figure 7, these particles tend to exhibit a Pd-rich surface layer that appears to be a few tens of nanometers thick.

Results of OSC measurements are listed in table 2. The measurements were performed immediately after aging, starting from low temperature (so that the Pd "reactivation" effect is not apparent [8]). For the single-metal catalysts made with ceria–zirconia (RhI, RhII and PdI), the OSC is significantly higher for Rh than Pd, and there is relatively little dependence on Rh loading, consistent

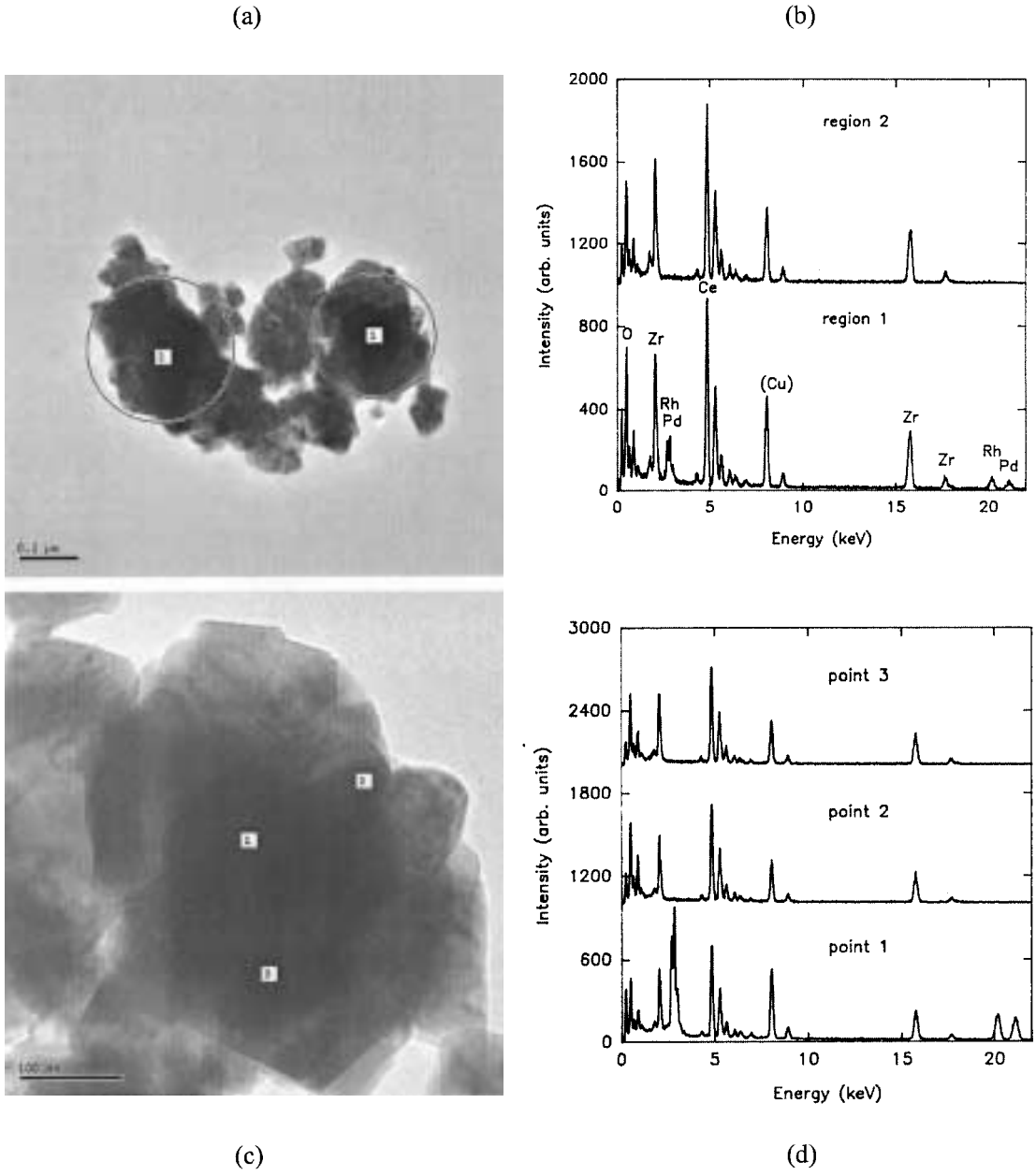

Figure 4. TEM image (a) and EDS results (b) obtained from PdI + RhII following the mild reduction treatment performed after aging. An enlargement of region 1 from (a) is shown in (c), together with corresponding EDS results (d). The probe size for the point analyses in (d) was 1 nm.

with previous observations [9]. For the bimetallic catalyst, PdI + RhII, the OSC falls between PdI and RhII, but it is clearly less than the average value, tending to be closer to PdI than RhII. Finally, the OSC of PdII + RhII is less than PdI + RhII, even though both are computed per gram of ceria–zirconia support.

4. Discussion

According to their equilibrium phase diagrams, both the Pt–Rh and Pd–Rh systems are immiscible at room temperature [10]. For temperatures above ~760 °C in the case of Pt–Rh and ~915 °C in the case of Pd–Rh, however, they form solid solutions, or random substitutional fcc alloys, where the lattice constants would be expected to have compositionally-weighted average values according to Vegard's Law. Once formed, such alloys may remain stable when quenched to lower temperatures.

The XRD result from PtI + RhI provides convincing evidence of alloy formation (and thus metal transport between initially distinct supports) during redox aging at 1050 °C. Since previous studies of both single-metal catalysts have shown that normal sintering processes under these conditions produce metal particles of the size found here (several tens of nanometers in diameter, on average) [11], it is apparent that the alloy particles

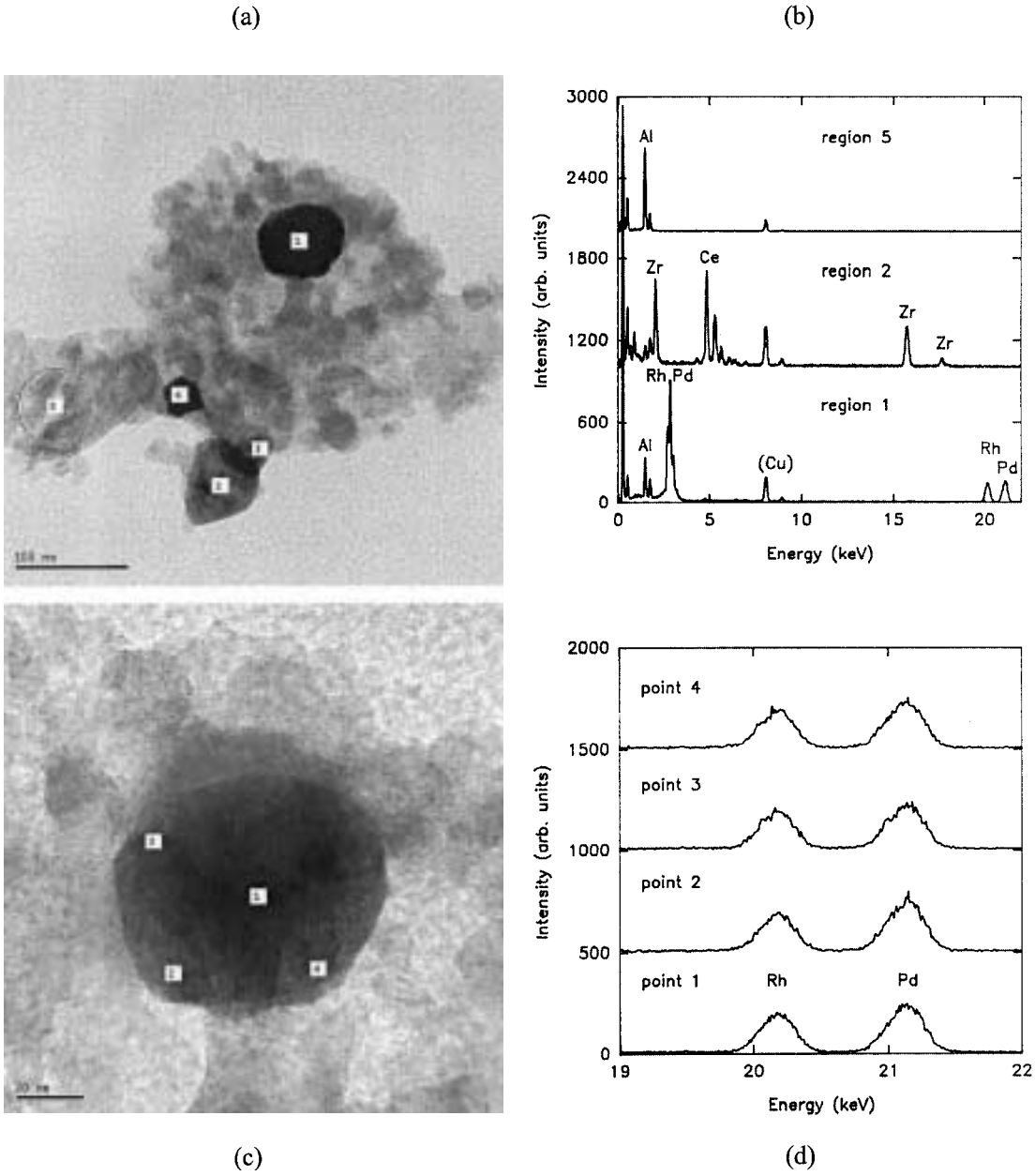

Figure 5. TEM image (a) and EDS results (b) obtained from PdII + RhII following the mild reduction treatment performed after aging. (Features 3 and 4 yield the same spectrum as region 2.) An enlargement of the precious-metal particle from (a) is shown in (c), together with corresponding EDS results (d). The probe size for the point analyses in (d) was 1 nm.

contain essentially all of the metal. It is not clear, however, whether transport of primarily one or both of the metals was involved. Vapor-phase transport of volatile oxides of Pt is known to occur relatively easily in an oxidizing environment [12], but sintering of the ceria–zirconia and agglomeration of individual grains, as illustrated by the TEM results, could have provided a path for the surface diffusion of either metal, as well. A recent study of mixed alumina-supported Pt and Rh catalysts also detected alloy formation, but only under reducing conditions and at a somewhat lower temperature, 900 °C [13]. In this case, it was suggested that primarily Pt had migrated across the boundaries of the ~6-μm alumina-powder particles comprising the single-metal catalyst supports.

The assessment of the Pd-containing bimetallic catalysts with regard to alloy formation is complicated, possibly by oxidization upon completion of the aging treatment (which ended with cooling to ~500 °C under flowing N_2, at which point the flow was stopped, allowing diffusion of room air back into the tube furnace). Although XRD provides little evidence of oxides, the peak, characteristic of an equimolar solid solution of Pd and Rh, on average, that results from the mild reduction treatment strongly suggests that alloying had occurred during aging. The TEM results also support

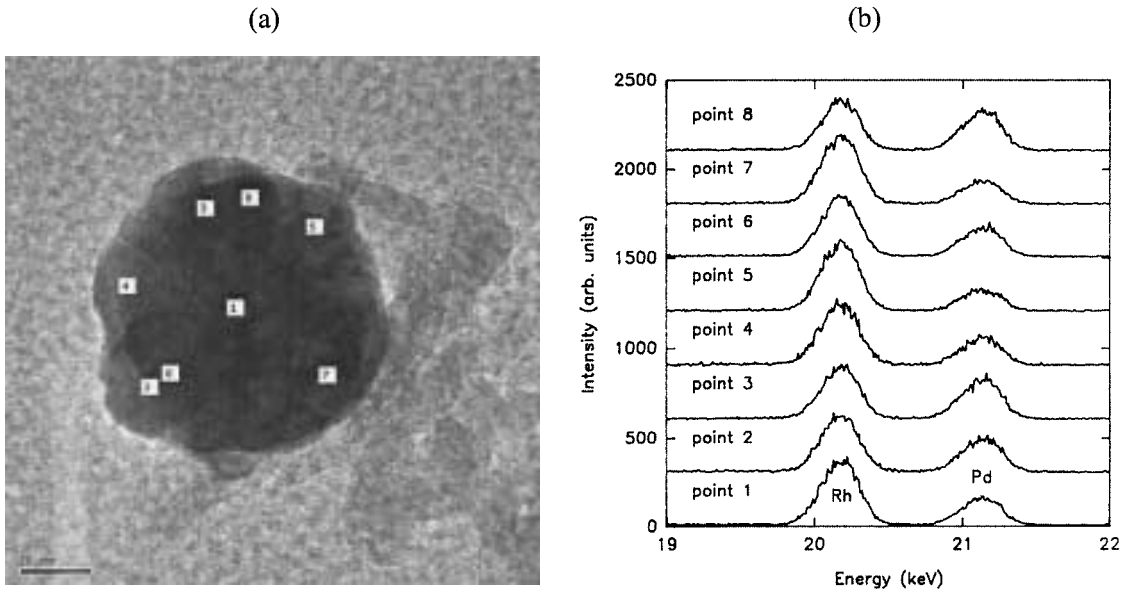

Figure 6. TEM image (a) and EDS results (b) of another precious-metal particle from PdII + RhII following the mild reduction treatment performed after aging. The probe size for the point analyses was 1 nm.

alloy formation, though with composition and homogeneity varying from particle to particle. In previous studies of the air oxidation of Pd-rich Pd–Rh alloy foil, it was found that PdO segregates onto the surface of the foil for temperatures up to nearly 800 °C, at which point $PdRhO_2$ forms [14,15]. Surface enrichment of alloy particles with Pd, observed by TEM in aged PdII + RhII after the 700 °C oxidation treatment, is consistent with this behavior. The failure to clearly observe PdO, $PdRhO_2$ or Rh_2O_3 by XRD may be due to a combination of low concentrations and poor crystallinities. It is thus surmised that Pd–Rh alloy particles formed during aging, but they then developed into highly defective partially oxidized particles during the cooling stage afterwards. The breadth of the alloy XRD peak, the presence of the small Rh (111) XRD peak, and the compositional inhomogeneity of the alloy particles observed by TEM all suggest that alloying in the Pd-containing bimetallic catalysts was probably not as complete as in PtI + RhI.

The formation, to at least some extent, of Pd–Rh alloy particles in both PdI + RhII and PdII + RhII

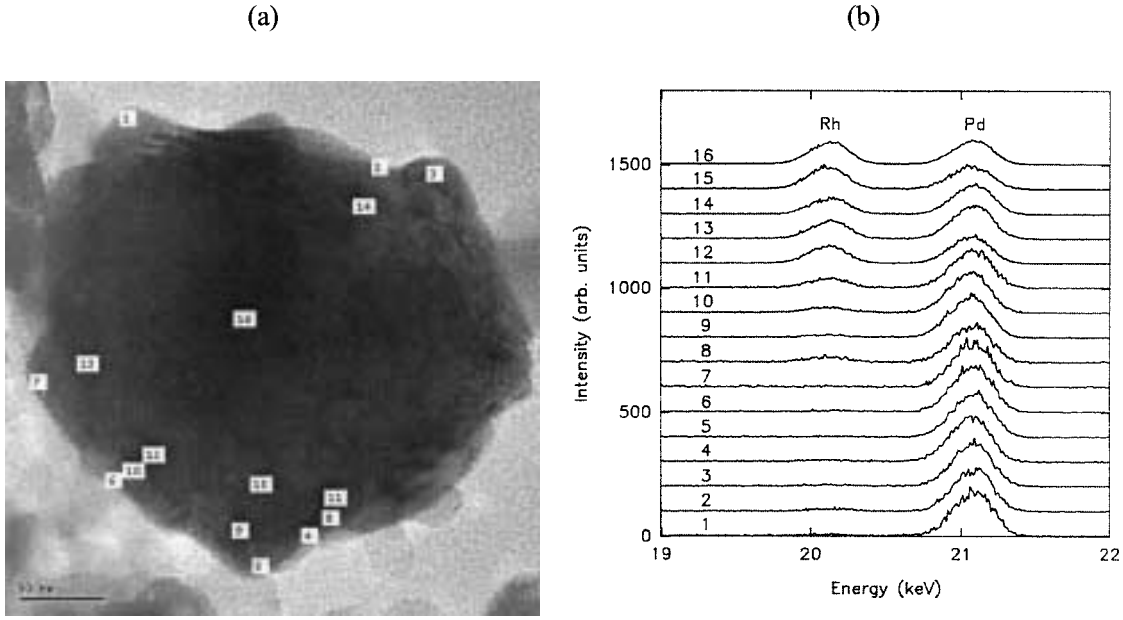

Figure 7. TEM image (a) and EDS results (b) of a relatively large precious-metal particle from PdII + RhII following the oxidation treatment (at 700 °C) performed after aging. The probe size for the point analyses was 1 nm. Note the gradient in the Rh/Pd ratio from the edge toward the center for each of the series: {2,14}, {4,8,11}, {5,9,15}, {6,10,12} and {7,13}.

Table 2
OSC (μmol O/g CZ3), using short pulses of 1% CO/0.5% O_2, after aging

Catalyst	Measurement temperature (°C)			
	250	300	350	500
RhI		67	200	
RhII		62	189	
PdI [a]	17	16	41	
PdI + RhII	19	28	68	541
PdII + RhII	15	22	33	376

[a] Using short pulses of 5% CO/2.5% O_2.

again leads to the conclusion that metal transport occurred between initially distinct supports during redox aging at 1050 °C. Surface diffusion is more likely to have been the principal mode of metal transport in these cases (though Pd also has a relatively high vapor pressure), but the alumina in PdII + RhII certainly endows this catalyst with a much higher surface area (and thus longer and more tortuous diffusion paths) than PdI + RhII. In view of the polycrystalline structure generally found in the large particles, their growth by migration and agglomeration of smaller particles also seems likely.

According to table 2, two distinct effects of metal transport on OSC may be identified. First, the OSC of PdI + RhII is much closer to that of PdI than RhII, suggesting that the alloy particles behave more like Pd than Rh. (Alternatively, the fact that the OSC of PdI + RhII is not a simple average of PdI and RhII is itself evidence for alloy particle formation.) This is consistent with the Pd enrichment of the surface of alloy particles following the oxidation treatment, observed by TEM. A similar loss of Rh character, though relative to NO reduction functionality, was found in early Pd–Rh bimetallic catalysts where alloy formation was suspected.

The second effect, apparent in PdII + RhII, is most likely associated with simple dilution. Based on the large difference in surface areas of alumina and ceria–zirconia after aging, only 10% of the Rh would remain on the ceria–zirconia after aging *if* Rh remained highly dispersed and its redistribution occurred completely and randomly. Of course, Pd could move the other way, from alumina to ceria–zirconia, but due to alloy formation with Rh, this should lower OSC, as in PdI + RhII. (Any Rh that moved to alumina but was not alloyed with Pd might be expected to undergo reaction with the alumina under high-temperature oxidizing conditions. This could account for the decrease in the Rh (111) XRD peak following the 800 °C oxidation treatment.) In fact, the metal dispersion is *not* high after aging, and a significant fraction of the ceria–zirconia particles have almost certainly lost all contact with metal particles, as shown in figure 5(a). A similar type of morphological effect on metal–ceria contact in a single-metal catalyst has recently been described [16].

5. Conclusions

This simple investigation of model bimetallic catalysts demonstrates that metal redistribution across support–particle boundaries can take place during high-temperature aging and, as a result, alloy formation and loss of OSC can occur.

Acknowledgment

The work at the University of Michigan was supported by National Science Foundation Grant DMR-9871177 (for the JEOL 2010F TEM, located in the Electron Microbeam Analysis Laboratory) and Ford Motor Company, through a University Research Program grant.

References

[1] H.-W. Jen, G.W. Graham, W. Chun, R.W. McCabe, J.-P. Cuif, S. Deutsch and O. Touret, Catal. Today 50 (1999) 309.
[2] G.W. Graham, H.-W. Jen, R.W. McCabe, A.M. Straccia and L.P. Haack, Catal. Lett. 67 (2000) 99.
[3] H.C. Yao, S. Japar and M. Shelef, J. Catal. 48 (1977) 111.
[4] H.C. Yao, H.K. Stepien and H.S. Gandhi, J. Catal. 61 (1980) 547.
[5] Y.-F. Yu-Yao and J.T. Kummer, J. Catal. 106 (1987) 307.
[6] J.S. Hepburn *et al*., Paper No. 941058, Society of Automotive Engineers, Warrendale, PA (1994).
[7] JCPDS files for Pt (04-0802), Pd (46-1043), Rh (05-0685), ceria–zirconia (38-1439), alumina (δ: 04-0877, θ: 11-0517), PdO (41-1107), Rh_2O_3 (41-541) and $PdRhO_2$ (27-1325).
[8] 17th North American Catalysis Meeting, "Modification of Oxygen-Storage-Capacities of Aged $Pd/Ce_{0.63}Zr_{0.37}O_2$ and $Rh/Ce_{0.63}Zr_{0.37}O_2$ Model Catalysts", Hung-Wen Jen, George W. Graham and Robert W. McCabe (unpublished).
[9] H.-W. Jen (unpublished).
[10] W.G. Moffat, *The Handbook of Binary Phase Diagrams*, vol. 5 (Genium Publishing Corporation, New York, 1984).
[11] G.W. Graham, H.-W. Jen, W. Chun and R.W. McCabe, J. Catal. 182 (1999) 228.
[12] P. Wynblatt and N.A. Gjostein, in: *Progress in Solid State Chemistry*, Vol. 9, eds. J.O. McCaldin and G. Somorjai (Pergamon Press, 1975) ch. 2.
[13] Z. Hu, F.M. Allen, C.Z. Wan, R.M. Heck, J.J. Steger, R.E. Lakis and C.E. Lyman, J. Catal. 174 (1998) 13.
[14] G.W. Graham, T. Potter, R.J. Baird, H.S. Gandhi and M. Shelef, J. Vac. Sci. Technol. A4 (1986) 1613.
[15] R.J. Baird, G.W. Graham and W.H. Weber, Oxid. Met. 29 (1988) 435.
[16] W.-J. Shen, A. Kobayashi, Y. Ichihashi, Y. Matsumura and M. Haruta, Catal. Lett. 73 (2001) 161.